International Research Journal of Innovations in Engineering and Technology (IRJIET)

ISSN (online): 2581-3048
Volume 10, Issue 2, pp 19-30, February-2026
https://doi.org/10.47001/IRJIET/2026.102004

Reducing Black Box Region in ESBMV: A Comparative Study of Frequency and Spatial Compounding

[1]Afnan Asaad, [2]Zainab R. Alomari

[1,2]Communication Engineering Department, College of Electronics Engineering, University of Ninevah, Mosul, Iraq

***Abstract* - Black Box Regions (BBRs), which represent a significant degradation of Eigenspace Based Minimum Variance (ESBMV) ultrasound imaging, occur mainly due to the result of phase decoherence and acoustic attenuation of heterogeneous media. These artefacts obscure clinically relevant anatomical features and thus destroy diagnostic precision. Although adaptive beamforming has advanced significantly, focused approaches for systematic BBR mitigation are still poorly examined. Accordingly, the current investigation assesses the restorative efficiency of non- multiplicative compounding techniques, namely Frequency Compounding (FC) and Spatial Compounding (SC), in reducing BBR artefacts. Performance assessment was done using Field II simulations and experimental phantom data measured by Speckle Signal minus Noise Ratio (SSNR) and Contrast to Noise Ratio (CNR). Findings prove that SC significantly outperforms FC in restoring the signal integrity of BBRs. By introducing angular diversity, SC effectively decorrelates speckle, especially at moderate steering angles. Conversely, while FC allows somewhat enhanced contrast improvement, the ability of the method to recover signal in areas of low coherence is limited. Collectively, these results show that incorporating SC into the ESBMV framework provides a powerful tool to reduce BBR artefacts and dramatically improve image fidelity for complex clinical applications.**

Keywords: Ultrasound Imaging, Black Box Region (BBR), Frequency Compounding (FC), Spatial Compounding (SC), Speckle Signal to Noise Ratio (SSNR).

I. INTRODUCTION

The growing need for high-resolution diagnostic ultrasound has led to the development of adaptive beamforming frameworks, in particular, Eigenspace-Based Minimum Variance (ESBMV) Beamformer [1]. By performing an eigen-decomposition of the covariance matrix to separate the signal and noise subspaces, ESBMV attains a lateral resolution that significantly outperforms that achievable with classical Delay-and-Sum (DAS) methods [2]. However, this improvement in resolution is accompanied by a significant price: a greater susceptibility to phase decoherence. This vulnerability is manifested in the form of Black Box Regions (BBR), localized artifacts where catastrophic signal suppression occurs in regions where the assumption of signal coherence is broken down [3].

Despite the fact that the clinical consequences of these aberrations are important and can complicate the visualization of important anatomic details, efforts in research have focused more on the overall image quality rather than on the specific restoration of signals within these dropout regions [4]. Notably, to our knowledge, there is an obvious lack of comparative studies evaluating non-multiplicative compounding approaches as a primary strategy for mitigation of BBR. Conventional coherence-based methods, including Coherence Factor (CF), are based on multiplicative weighting schemes, which tend to make the BBRs worse due to the unequal penalty on low-coherence signals [5].

This work fills an important research gap by systematically exploring Spatial Compounding (SC) and Frequency Compounding (FC) as "restorative" methodologies, rather than merely "additive" methodologies. Unlike multiplicative approaches, these compounding strategies are based on an attempt to recover suppressed signal energy in BBRs by bringing in angular or spectral diversity, hence stabilizing the covariance matrix. The current work assesses the effectiveness of the techniques in improving Speckle Signal,-to-NOI (SSNR), and increasing the reliability of the diagnosis, while maintaining the excellent lateral resolution of the ESBMV system.

II. RELATED WORK

Adaptive beamforming and compounding techniques have been widely researched to improve ultrasound image resolution and contrast, however, the ever-present Black Box Regions (BBRs) in Eigenspace Based Minimum Variance (ESBMV) imaging still remain poorly addressed.

Spatial and frequency compounding have long been known to be successful global enhancement strategies. Montaldo et al. (2009) [16] showed that coherent angular compounding is an improvement over contrast and resolution in the form of partially decorrelated plane-wave averaging. Li et al. (2018) [14] found effective speckle suppression with frequency compounding at the cost of axial resolution. Despite these improvements, both approaches were evaluated mostly

ISSN (online): 2581-3048
Volume 10, Issue 2, pp 19-30, February-2026
https://doi.org/10.47001/IRJIET/2026.102004

by global image metrics with no explicit investigation of localized signal recovery within BBRs.

The ESBMV beamformer proposed by Asl and Mahloojifar (2010) [7] greatly enhanced lateral resolution and contrast by applying adaptive weights to a small signal subspace. However, the method itself has an inherent mechanism that suppresses low energy, or decorrelated, signals, which later turned out to be BBR artifacts. Although the overall image quality improved, some dark areas were not quantified or reduced in their effect.

Subsequent studies tried artifact reduction through post processing and coherence weighting. Zeng et al. 2012 [17] combined ESBMV and Wiener filtering, but the global nature of post-filter failed to cope with localized BBR suppression. Rindal et al. (2017) [10] provided a systematic analysis of dark-region artifacts and placed the formation of BBRs as a result of covariance instability as opposed to physical attenuation, but did not suggest any direct recovery mechanism.

Coherence-based extensions of ESBMV were later provided. Wu et al. (2017) [18] and Wang et al. (2017) [19] included smoothed coherence factors and Short-Lag Spatial Coherence (SLSC), respectively. Although contrast and clutter rejection improved, their multiplicative weighting schemes further attenuated low coherence signals, limiting effective restoration within BBR regions.

Region aware frameworks started to come up which can overcome these limitations. A strategy for modulating eigenspace projection and increasing uniformity was proposed by Alomari (2017) [20] using adaptive region discrimination. Lan et al. (2021) [9] proposed adaptive eigenvalue thresholding, and covariance-based adaptive weighting was proposed in [5] to improve the robustness. Thanoon et al. (2023) [28] further emphasized spatially adaptive enhancement in ultrafast imaging. While these approaches did enhance stability and contrast, they usually involved resolution-charge trade-offs and did not provide a rigorous region-specific quantitative evaluation (e.g., SSNR within BBRs).

More recent investigations continued to focus on world improvements. Shen et al. (2024) [13] showed the improvement of speckle uniformity when increasing angular diversity, but used global metrics. Zhao et al. [3] suggested an adaptive coherence-based post-filter, but its multiplicative property limited energy recovery in seriously degraded areas. Hasegawa (2024) [1] pointed out that covariance instability and dark-region artifacts are unsolved problems of ultrafast ultrasound systems. Li et al. [8] investigated frequency-domain eigenspace projection for robustness enhancement but did not explicitly focus on BBR recovery.

In summary, in spite of the extensive research in adaptive beamforming, coherence weighting and compounding techniques [21], the explicit and quantitative recovery of Black Box Regions in ESBMV imaging using non-multiplicative compounding strategies is insufficiently researched. In particular, a controlled comparison between Spatial Compounding (SC) and Frequency Compounding (FC) as physical mechanisms for covariance stabilization and localized signal restoration, has not been fully addressed. This gap is the motivation of the present study.

III. BACKGROUND METHODS

3.1 Minimum Variance (MV) Beamforming

The Minimum Variance (MV) beamformer improves image resolution and suppresses interference by adaptively determining weights that minimize output power while preserving unity gain in the focal direction [13], [14]. This is expressed as the subsequent optimization problem [3]:

$$W_{MV} = arg \min_{W} W^H R W \qquad (1)$$

$$subject\ to\ W^H a = 1,$$

where w represents the adaptive weight vector, R denotes the covariance matrix of the received data, and a signifies the steering vector. The optimal weighting vector is given by [6]:

$$W_{MV} = \frac{R^{-1}a}{a^H R^{-1} a} \qquad (2)$$

In practice, R is unknown and necessitates estimation from the received signals. To guarantee the invertibility of the matrix and to enhance robustness, spatial smoothing is employed by partitioning the array of M elements into P overlapping subarrays of length L , where P = M - L + 1. Temporal smoothing over K snapshots is integrated . The estimated covariance matrix , denoted as $\hat{R}$, is articulated as [3], [15]:

$$R = \frac{1}{P}\sum_{P=0}^{P-1} G_p G_p^H, \qquad (3)$$

where Gp(n) represents the p-th subarray data vector at time n:

$$G_p = [y_p(n) y_{p+1}(n) \quad \dots \quad y_{p+Lp-1}(n). \qquad (4)$$

The beamformer output is then calculated as the inner product of the weight vector and the averaged subarray data:

ISSN (online): 2581-3048
Volume 10, Issue 2, pp 19-30, February-2026
https://doi.org/10.47001/IRJIET/2026.102004

$$Y = w_{MV}\frac{1}{P}. \quad (5)$$

The selection of subarray length L is a critical design trade-off; while a larger L enhances resolution and contrast by improving covariance estimation accuracy, it may increase computational complexity and degrade background speckle uniformity [9], [16].

3.2 Eigenspace-Based Minimum Variance (ESBMV)

The Eigenspace-Based Minimum Variance (ESBMV) beamformer is an advanced variant of the MV method designed to improve robustness against covariance estimation errors and enhance contrast [1], [9]. The core of this technique is the eigen-decomposition of the estimated covariance matrix $\hat{R}$ into orthogonal subspaces:

$$R = \vee \wedge \vee^{H} = \sum_{i=1}^{LP} \lambda_i \upsilon_i v_i^H, \quad (6)$$

where $\wedge$ = diag [$\lambda_1 \geq \lambda_2 \geq \ldots \geq \lambda_{Lp}$] contains the eigenvalues in descending order, and υ contains the corresponding eigenvectors. The ESBMV algorithm partitions these into a signal subspace (E_S) and a noise subspace (E_n) using an adaptive threshold λ_{th} [1]:

$$\lambda_{th} = \lambda_1 . \delta, \quad (7)$$

where $\delta$is the user-defined parameter $\delta \in$ [0, 1] that controls the classification sensitivity. A higher δ value limits the signal subspace to only the most dominant eigenvectors, which sharpens resolution but may trigger Black Box Region (BBR**)** artifacts in low-SNR areas due to excessive signal rejection. Conversely, a lower δ includes more eigenvectors in E_S, improving speckle uniformity and robustness at the expense of resolution [9], [10]. The signal subspace projector is constructed as:

$$P_s = \sum_{i=1}^{N_{sig}} v_i v_i^H \quad (8)$$

where N_{sig} is the number of eigenvalues exceeding λ_{th}. The final ESBMV weight vector is obtained by projecting the standard MV weights onto this signal subspace [1], [6]:

$$W_{ESBMV} = p_s w_{MV} \quad (9)$$

The systematic procedure for this subspace decomposition and the separation of signal and noise components is detailed in the flowchart shown in Figure (1).

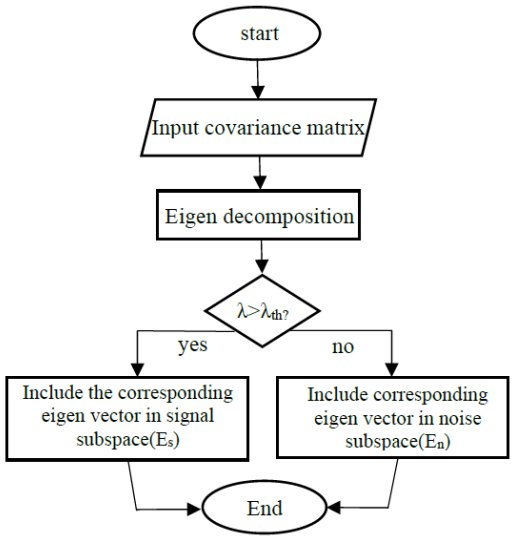

Figure 1: A flow chart showing the decomposition operation of the covariance matrix in ESBMV

3.3 Black Box Region (BBR) Artifacts in ESBMV

Despite the better resolution of the ESBMV methodology, it is still prone to the Black Box Region (BBR), which is characterized by localized voids in the signal, especially in low signal-to-noise ratio or decorrelated regions [3], [9]. Unlike physical attenuation, the BBRs are artificially introduced from the algorithmic point of view; they arise from the fact that the eigenvalues of the covariance matrix are decreasing as a result of weak echoes and leading to misclassification of true signals as noise in eigenspace projections and their consequent suppression [3]. The severity of BBRs is controlled by the threshold parameter δ. An increased d results in an increased resolution; however, simultaneously it leads to an increased amplification of BBRs due to the over-suppression of weak signal constituents [9].

Contemporary mitigation strategies have mostly used multiplicative schemes based on coherence [4], [7] - such as CF, GCF, and SLSC. Nevertheless, these approaches often make BBRs worse by further reducing low-coherence regions. As a consequence, non-multiplicative methods, such as spatial and frequency compounding, exploiting the angular and spectral diversity to stabilise the statistics of the signal and to increase the visibility in these areas, are increasingly recommended [14], [17].

3.4 Frequency Compounding in Ultrasound Imaging

Frequency compounding (FC), a time-honored decorrelation approach, has been consistently adopted to reduce the speckle noise by exploiting the frequency-dependent morphology of ultrasonic interference patterns [14], [15]. The basic principle of this technique is to divide the wide bandwidth of the received radio frequency (RF) signal into a

ISSN (online): 2581-3048
Volume 10, Issue 2, pp 19-30, February-2026
https://doi.org/10.47001/IRJIET/2026.102004

sequence of sub-bands with center frequencies on different frequency echelons. This stratification gives rise to a collection of constituent images that are each characterized by partially decorrelated speckle textures. By averaging these sub-band images in the following steps, the stochastic constructive and destructive interferences can be effectively suppressed, and the resulting enhanced contrast and more homogeneous background can be achieved [18].

Within the ESBMV framework, the main goal of FC is to stabilize covariance matrix estimation by diversifying the spectral content of the input data. While traditional FC provides an inevitable trade-off, in which the reduction in speckle is offset by a reduction in axial resolution due to the narrower bandwidth of each sub-band [14], its specific effectiveness for reducing Black Box Region (BBR) artefacts has not previously been investigated in academic literature. The present study, therefore, interrogates the question of whether the spectral diversity proffered by FC can forestall the eigenvalue shrinkage that typically precipitates signal over-suppression in adaptive beamforming.

3.5 Spatial Compounding in Ultrasound Imaging

Spatial compounding (SC) dramatically improves image fidelity by the coherent combination of several acquisitions that are acquired under different steering geometries [16, 17]. Such angular diversification engenders speckle formations and phase-correlated aberrations - colloquially referred to as BBRs that manifest heterogeneously across the individual datasets. By combining these decorrelated views, the algorithm manageably interpolates for the deficient signal content of the signal and reduces the malicious interference that would have otherwise led to the excessive suppression of signals within the framework of adaptive beam-forming.

In the context of the ESBMV paradigm, SC acts as a powerful stabilizer of the statistics of the signal. Unlike multiplicative filtering approaches, SC provides a refined estimate of the covariance matrix and hence recovers the information that was lost. Consequently, this study brings the focus on SC as an important non-multiplicative methodology to attenuate BBRs, which so far have been largely underappreciated in the existing adaptive beamforming literature.

IV. PROPOSED STUDY

The present study discusses the effectiveness of two different compounding strategies to mitigate BBR artifacts in the ESBMV framework. The evaluation is done by two main test cases that are devised to test the trade off between BBR suppression, contrast enhancement, and resolution preservation.

Scenario 1: Frequency Compounding (FC) Configuration. In the primary configuration, frequency compounding was used by splitting the broadband signal into three distinct sub-bands in each insonification. A severe systematic question of the different frequency combinations was undertaken to determine the spectral amalgamation that provides the best restoration of the BBR. The analysis focused on the enhancement of spectral diversity as a way to strengthen the stability of the signal in the BBR domain, at the same time tracking the inevitable axial resolution degradation that is associated with this process.

Scenario 2: Spatial compounding with 2 different experimental arrangements:

1. Angular Spacing Analysis: A predetermined set of three insonification angles was used and the angular spacing between the insonification was varied to find the minimum angular decorrelation required to totally eliminate the BBR artifacts.

2. Angular Density Analysis: By analyzing aggregate count of compounded angles, this configuration determined that the saturation level beyond which the additional angular information does not produce any more improvement in BBR suppression or Speckle Signal versus Noise Ratio (SSNR).

V. SIMULATION SETUP AND DATASETS

In the face of the lack of real clinical data covering both FC and SC gained under the same conditions, we have created an entirely fake data set that will be used with the Field II platform. Empirical investigations often highlight discrepancies caused by differences in imaging equipment, transducer settings or even scanning modes since systematic biases are introduced that destroy the integrity of inter-method comparisons. In this regard, to overcome these challenges and maintain a stringent, regulated test, all of the experiments described in this paper were conducted in the framework of a disinfected, sterile simulation environment.

The computational environment was carefully constructed to simulate real ultrasound imaging while ensuring free control over all the variables - speckle phenomenology, geometrical configuration, and transducer characteristics - all told. A customised cystic phantom was created in Field II. The phantom consists of background scatterers, anechoic and hyperechoic cystic formations, and discrete point targets at various depths. Such a construct enables a rigorous appraisal of contrast, resolution, and speckle dynamics under repeatable and unvaried conditions. The suite of beamforming and compounding algorithms (MV, ESBMV, FC, and SC) was each realised in the MATLAB software.

International Research Journal of Innovations in Engineering and Technology (IRJIET)

ISSN (online): 2581-3048

Volume 10, Issue 2, pp 19-30, February-2026

https://doi.org/10.47001/IRJIET/2026.102004

An additional man-made phantom, designed in Field II, was made to reflect a well-controlled imaging environment. Its background was characterised by homogenous speckle with scatterers stochastically distributed in a volumetric expanse extending from between 20-100mm in depth, -5-5mm in elevation, and -15-15mm laterally. The amplitudes of these background scatterers were in a Gaussian ensemble.

Within this phantom, two cystic lesions were placed: the first one was a 2 radius hyperechoic cyst located at 65 mm depth with acoustic amplitudes increased by +30 dB to mimic high echogenicity; the second one was a 3 radius anechoic cyst located at 35 mm depth and 3 mm laterally with nullified scatterer amplitudes. In addition, a quartet of point scatterers, which were used as high-intensity resolution benchmarks, were placed at depths of 30, 40, and 50 mm, all laterally aligned at -5 mm.

Simulation was done using a 128-element linear array transducer, centred at 3 MHz with a sampling frequency of 100 MHz. The velocity of propagation was fixed at 1540 m s -1 (congruent with canonical soft tissue acoustics). Such parameter selections were judiciously chosen in order to harmonise the simulated scenario with the conventional clinical imaging praxis.

VI. QUALITY METRICS

We used three quantitative measures namely the speckle signal-to-noise ratio (SSNR), the contrast-to-noise ratio (CNR) and the full width at half maximum (FWHM) to compare the efficacy of Feature Compression (FC) and Super-realistic Compression (SC).

Altogether, these measurements yield the overall evaluation of the ability of each method to reduce the degree of speckle noise, increase the contrast, and retain the image resolution [19].

The SSNR was also computed in order to measure the change in tissue visibility, especially in the bounded-by-regression (BBR) area and the surrounding background. This measure is used to assess the quotient of the mean signal intensity divided by the measure of deviation of the background noise in a specified region of interest as stated in the expression below [19, 22]:

$$SSNR_{Bg} = \frac{\mu_{Bg}}{\sigma_{Bg}}, \quad (10)$$

where μ_{Bg} represents the mean signal intensity in the region of interest, and σ_{Bg} is the standard deviation representing the speckle noise level. In the experimental setup, the BBR region was assessed within a rectangular area of approximately 7 mm², while the background region was taken for an area of approximately 6 mm². $SSNR_{BBR}$ is measured using [22]:

$$SSNR_{BBR} = \frac{\mu_{BBR}}{\sigma_{BBR}}. \quad (11)$$

The contrast ratio (CR) assesses contrast by measuring the absolute difference between the mean intensity within the cyst and the surrounding background. It is calculated as [21]:

$$CR = |\mu_i - \mu_b|, \quad (12)$$

where the mean values within the cyst target and speckle are μ_i and μ_b, respectively. CNR is another measure of contrast that is found as follows [21]:

$$CNR = \frac{|\mu_{i-}\mu_b|}{\sqrt{\sigma_i^2 + \sigma_b^2}}. \quad (13)$$

In this study, SSNR was measured within a rectangular area of approximately 7 mm², positioned over the acoustically degraded zone in the B-mode image. This metric quantifies the signal clarity and speckle suppression within the BBR.

The full width at half maximum (FWHM) represents the lateral resolution and is defined as the width of the signal's main lobe at the point where the amplitude drops to half of its maximum value [20]. Lower FWHM values indicate sharper lateral resolution. The FWHM is obtained by calculating the main lobe's FWHM (6-dB beamwidth) in the lateral direction [19],[22].

VII. RESULT

7.1 Simulation Results

In order to carefully examine the improvement of Beam-related Back-scatter (BBR) artifacts in a carefully controlled acoustic environment, we created a numerical cyst phantom using the Field II simulation environment. The phantom consisted of a hypoechoic cyst (3 mm radius) placed at 35 mm, a hyperechoic cyst (2 mm radius) placed at 45 mm, and 3 point scatterers embedded at depths of 30, 40, and 50 mm to be used as resolution reference. A 128-element linear array was modelled with a center frequency of 3 MHz, that simulate the experimental parameters.[23]

Figure 2 is an example of the qualitative influence that comes from augmenting the angular diversity upon BBR mitigation in the context of SC - ESBMV. In contrast to the conventional ESBMV baseline (Fig. 2b), which shows a significant reduction in signal level in deeper regions, the reconstructions estimated by the SC-integrated scheme (Figs. 2c-e) show a progressive supply of continuity of the speckles.

International Research Journal of Innovations in Engineering and Technology (IRJIET)

ISSN (online): 2581-3048

Volume 10, Issue 2, pp 19-30, February-2026

https://doi.org/10.47001/IRJIET/2026.102004

Though the narrow angular increment of 10^o allows for only partial mitigation (Fig. 2c), by increasing the separation to 20^o (Fig. 2d) and then 30^o (Fig. 2e) allows for a considerable improvement in inter-angle decorrelation. The 30° configuration ultimately achieves the best BBR suppression with a structural visibility and background uniformity reinstatement while preserving the integrity of point-target responses.

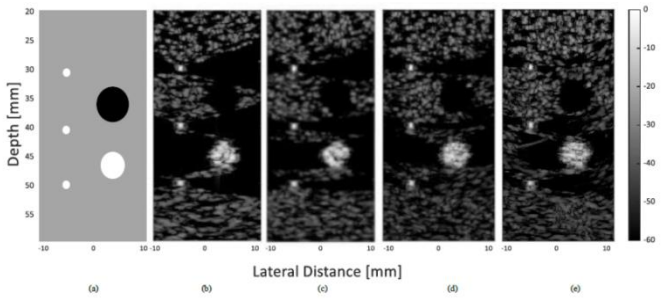

Figure 2: constructed phantom images. (a) Phantom schematic. SC at (b) 0°, (c) ±10°, (d) ±20°, (e) ±30° (60 dB dynamic range)

The results related to FC-ESBMV are represented in Figure 3. Despite the fact that FC engenders conspicuous speckle attenuation and texture refinement, its feasibility in BBR recovery is comparatively constrained when compared to SC. Reconstructions from narrow (1-3-5MHz) and lower-frequency (1-2-3MHz) sub-bands arrangements (Figs.3c-d) allow only limited restitution of signal in dark regions. Even with the maximal spectral separation (1-5-9 MHz) shown in Fig. 3e, which is ostensibly maximizing spectral diversity, the BBR is conspicuous. This indicates that while FC is successful in improving the overall smoothness of an image, it is not as successful as SC in forestalling the algorithmic signal rejection characteristic of ESBMV for these specific artifacts.

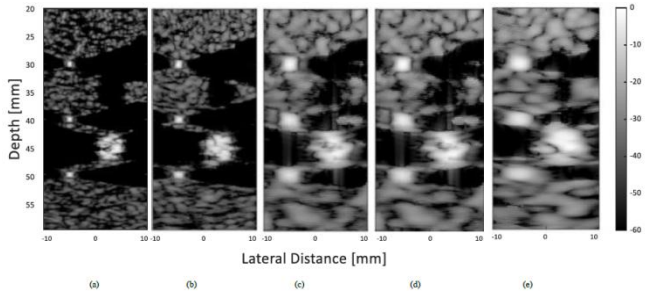

Figure 3: Constructed phantom images. (a) ESBMV (no FC), (b) (2,4,6), (c) (1,3,5), (d) (1,2,3), and (e) (1,5,9) mhz. 60 dB dynamic range

To objectively assess the performance of Spatial Compounding (SC) in reducing the effect of the artifacts in the Black Box Region (BBR), we extracted various key performance indicators from the simulated cyst phantom. These include the Speckle Signal-to-Noise Ratio (SSNR) in both the BBR and its background, Contrast-to-Noise Ratio (CNR) and Full Width at Half Maximum (FWHM) measured at two depths (30 mm and 40 mm) to measure the lateral resolution. Table 1 shows these metrics for a number of angular configurations compared with the baseline ESBMV.

Table 1: SC Performance Metrics Using Simulated Cyst Phantom

Compounded Angles	SSNR at BBR	SSNR at Background	CNR	FWHM (30mm)	FWHM (40mm)
ESBMV	0.26	0.78	1.42	0.39	0.47
(-5°, 0°, 5°)	0.24	0.69	1.40	0.38	0.49
(-10°, 0°, 10°)	0.22	0.69	1.34	0.37	0.46
(-15°, 0°, 15°)	0.28	0.69	1.36	0.35	0.42
(-20°, 0°, 20°)	0.37	0.71	1.29	0.32	0.42
(-25°, 0°, 25°)	0.51	0.71	1.32	0.31	0.38
(-30°, 0°, 30°)	0.54	0.73	1.25	0.31	0.46

To further emphasize the restoration capability, Figure 4 provides a direct comparison between the baseline and the optimized SC-ESBMV (5 angles, 15° steps).

This comparison highlights that spatial diversity effectively "fills in" the BBR-related voids, providing a more reliable representation of the underlying tissue anatomy.

The synergistic integration of Spatial Compounding (SC) with ESBMV provides a robust solution to the persistent challenge of Black Box Region (BBR) artifacts. As demonstrated qualitatively in Figure 4 and quantitatively in Table 1, the proposed methodology achieves a dual benefit: effectively reinstating the suppressed signal energy within the BBR—evidenced increase in SSNR (from 0.26 to 0.54)—while simultaneously enhancing lateral resolution, with a 20% improvement in FWHM.

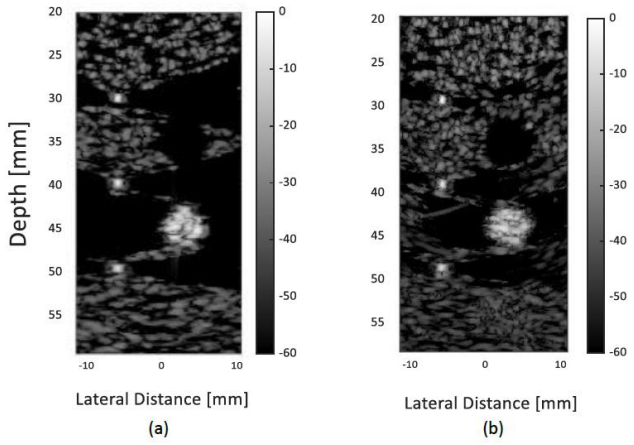

Figure 4: Constructed phantom images using (a) ESBMV (δ = 0.3, *Lp* = 16), (b) SC (step = 15 °, no.of angles=5). All images are shown in a dynamic range of 60 dB

International Research Journal of Innovations in Engineering and Technology (IRJIET)

ISSN (online): 2581-3048

Volume 10, Issue 2, pp 19-30, February-2026

https://doi.org/10.47001/IRJIET/2026.102004

Unlike conventional multiplicative weighting techniques, which demonstrate inferior performance in low-coherence regions, the angular diversity offered by the ±30° configuration supplies the necessary decorrelation to ensure the stability of covariance matrix estimation. These findings confirm that SC-ESBMV not only addresses artificial signal voids but also maintains the high-resolution integrity of adaptive beamforming, thus establishing itself as a superior candidate for high-quality ultrasound imaging in acoustically challenging environments.

7.2 In Vitro Dataset Results

The experimental phantom dataset offered by the Plane-wave Imaging Challenge in Medical Ultrasound (PICMUS) [25] was obtained with a Vantage 256 research scanner (Verasonics Inc., Kirkland, WA) and a L11-4v linear array transducer, imaging a multi-purpose tissue mimicking phantom (CIRS Model 040GSE). This phantom has been intentionally designed to test contrast and resolution abilities and includes high contrast wire targets and hypoechoic cystic inclusions.

The speckle correction technique was tested on the in-vivo experimental data set with two threshold values, δ = 0.3 and δ = 0.2, at angular steps of 5o, 10o and 15°. The qualitative results for δ = 0.3, shown in Figure 5, show the progressive recovery of the speckle texture in the Black Box Region (BBR). While the baseline ESBMV (Figure 5b) has severe signal dropout, adding angular diversity in Figures 5c-e stabilizes the covariance matrix well enough for the adaptive beamformer to restore structurally suppressed information.

The quantitative impact of this configuration is summarized in Table 2 (δ = 0.3).

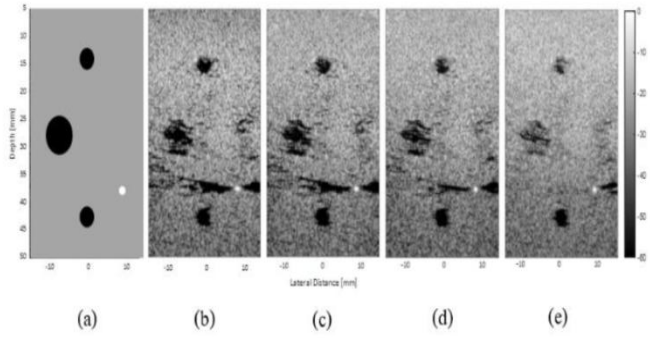

Figure 5: In vitro images using SC-ESBMV of the contrast dataset using with δ = 0.3, no. of compounded angles=3 and different angular steps: (a) A Schematic Diagram Of CIRS Ultrasound Phantom (b) 0°, (c) 5°, (d) 10°, (e) 15. All images are shown in a dynamic range of 60 dB

where the SSNR within the BBR rose from a baseline of 2.89 to a peak of 4.72 at a 15° step. This demonstrates that even with a more conservative threshold, moderate angular compounding significantly enhances signal recovery in low-SNR areas.

Table 2: SC-ESBMV at δ = 0.3 using different angular steps, no. of compounded angles=3

Angular Step	SSNR at BBR	SSNR at Background	CNR	FWHM
0° (PWI)	2.89	3.39	5.54	0.79
5°	3.15	2.63	4.95	0.74
10°	3.19	3.14	4.06	0.68
15°	4.72	2.74	3.01	0.56

This qualitative recovery is further explored in Figure 6, which presents the results for the lower threshold of δ = 0.2.

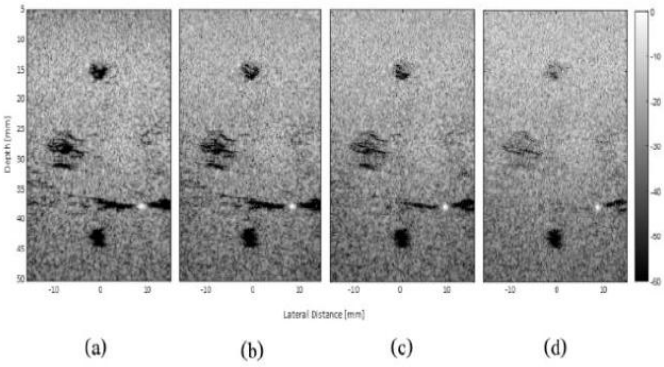

Figure 6: Experimental images using SC with δ = 0.2, no. of compounded angles=3and different angular steps: (a) 0°(single angle), (b) 5°, (c) 10°, (d) 15°, all images are shown in a dynamic range of 60 dB

The corresponding quantitative measurements for the δ = 0.2 configuration, further detailing the impact of angular diversity on BBR restoration and image quality, are compiled in Table 3.

Table 3: SC-ESBMV at δ = 0.2 using different angular steps, no. of compounded angles=3

Angular Step	SSNR at BBR	SSNR at Background	CNR	FWHM
0°	2.71	3.45	4.16	0.79
5°	2.81	3.38	3.44	0.75
10°	3.31	3.13	2.76	0.60
15°	4.79	2.72	1.96	0.56

To synthesize the relationship between the threshold parameter δ and the angular compounding steps, Figure 7 presents a comparative analysis of the performance trends for both δ = 0.3 and δ = 0.2. The curves clearly illustrate that as the angular step increases, the SSNR within the BBR follows a consistent upward trajectory for both cases, confirming that angular diversity is the primary driver for signal restoration.

ISSN (online): 2581-3048
Volume 10, Issue 2, pp 19-30, February-2026
https://doi.org/10.47001/IRJIET/2026.102004

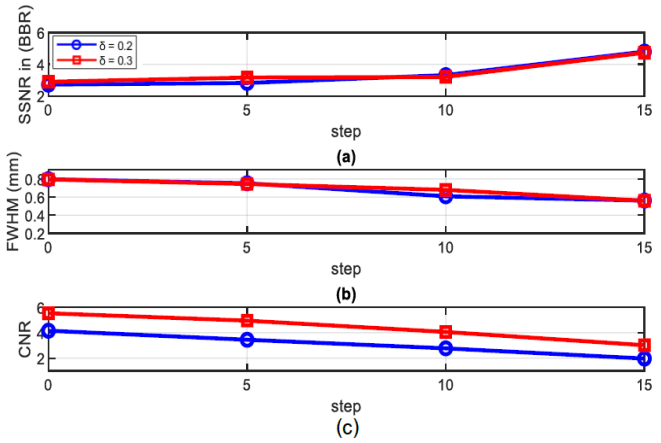

Figure 7 : (a) Variation of SSNR measured within BBR, (b) variation of FWHM, and (c) variation of CNR as functions of the angular step for δ = 0.2 and δ = 0.3

Nonetheless, Figure 7 simultaneously shows the difference in contrast performance; the CNR curve for δ = 0.2 shows a significantly steeper performance with reference to the curve for δ = 0.3. This graphical representation highlights the extreme sensitivity of the ESBMV algorithm to the value of threshold selected, in the sense that a smaller value of δ places greater emphasis on signal recovery at the cost of contrast fidelity. In contrast, the FWHM curves for the two configurations converge at the 15° step thereby strengthening the conclusion that the resolution improvement provided by spatial compounding retains its robustness and is independent of the subspace thresholding level.

In sum, these comparative trends provide a transparent decision-making process for ultrasound beamforming: δ = 0.3 is better for general imaging, where contrast is the major diagnostic visibility criterion, while δ = 0.2 is justified in those purposes where BBR suppression is the most important diagnostic visibility criterion.

Beyond the consideration of angular spacing, investigation has considered the influence of the number of compounded angles (N = 1, 3, 5, 7) on the image quality while keeping the angular step constant. The qualitative progression is shown in Figure 8, while the corresponding quantitative metrics are compiled in Table 4.

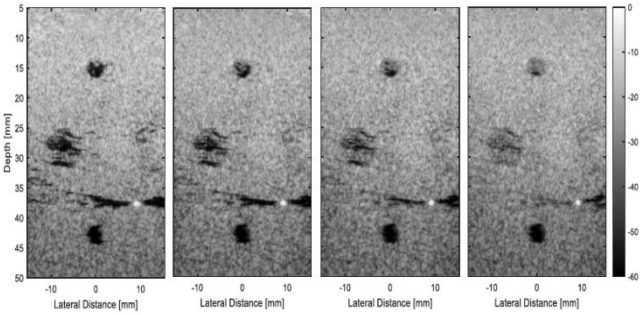

Figure 8: Experimental images showing the effect of `increasing the number of compounded angles with (δ = 0.3) (Step = 5°): (a) 1 angle, (b) 3 angles, (c) 5 angles, (d) 7 angles. All images are shown in a dynamic range of 60 dB

The quantitative data in Table 4 confirms the qualitative observations in Figure 8, highlighting that increasing the number of compounded angles to N=7 provides the most robust suppression of BBR artifacts. While the resolution (FWHM) consistently improves with higher angular density, the noticeable decline in CNR suggests that N=7 represents a critical threshold where signal restoration is maximized before excessive angular averaging begins to degrade structural contrast.

Table 4: SC-ESBMV at δ = 0.3 using different no. of compounded angles, angular steps, =5

Angular Step	SSNR at BBR	SSNR at Background	CNR	FWHM (mm)
1	2.81	3.15	4.62	0.8
3	2.816	3.38	3.44	0.74
5	3.35	3.41	2.6	0.64
7	4.89	3.4	2.1	0.56

7.3 Clinical Carotid Artery Results

Within the context of seeking strict validation of clinical efficacy of the SC -ESBMV framework, this study has now shifted away towards controlled phantom experimentation towards an examination of a bona fide human carotid artery dataset, as cited in reference [26]. This specific data has become a gold standard in the ultrasound research community, due to the particular mixture between the extremely reflective vessel walls and the attenuated arterial lumen. These conditions, with strong artifacts associated with bulk-motion (BBR) and phase aberration, present a formidable challenge to any reconstruction algorithm consequently providing an invaluable testbed in evaluating the robustness of the approach to physiologically realistic perturbation, principally, heterogeneity of tissues and minimal patient motion.

International Research Journal of Innovations in Engineering and Technology (IRJIET)

ISSN (online): 2581-3048

Volume 10, Issue 2, pp 19-30, February-2026

https://doi.org/10.47001/IRJIET/2026.102004

The following subsection outlines the fidelity results of the exemplary image achieved through the application of SC-ESBMV scheme that utilizes N=7 angular planes and aperture parameter of 7= -0.3, which is compared to the traditional ESBMV baseline. Compared to previous phantom experiments that shed light on the effects of angular density and interscan spacing on the quality of images, the current in-vitro experiment aims at proving the restorative ability of the algorithm as a whole. To this end, we provide a typical example of the evidence of total suppression of BBR artifacts in a real clinical setting.

Figure 9 gives a summary of the qualitative improvement made; a side-by-side comparison is an irrefutable evidence of the better vascular architecture demarcation the proposed technique offers.

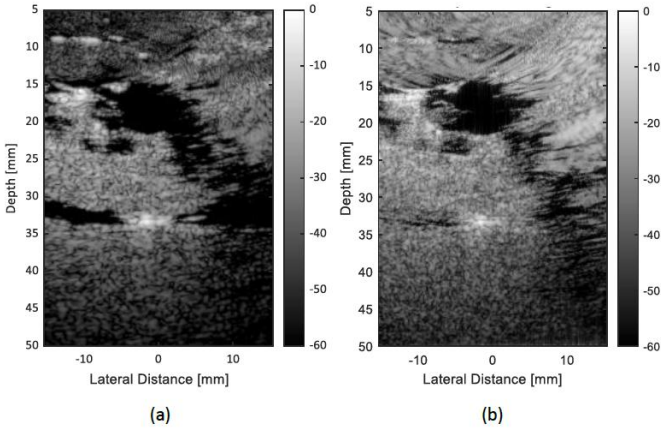

Figure 9: In-vivo B-mode images of the human carotid artery: (a) Baseline ESBMV (δ = 0.3) suffering from BBR artifacts near the vessel walls, and (b) Enhanced SC-ESBMV (N=7, δ = 0.3) showing restored speckle integrity and clearer boundary definition

As Figure 9 shows, the SC-assisted framework is capable of filling the artificial signal voids (BBR) that conceal vessel boundaries in the standard ESBMV. The lumen of the arteries thus becomes more homogenous and structural continuity of the carotid wall is significantly increased. This result supports the conclusions of the phantom experiments, i.e. the imperative of angular diversity and also proves that the same results can be directly applied in complex clinical imaging. To this end, the method becomes more diagnostic with no loss in the much needed anatomical detail.

VIII. RESULT

The SC-assisted ESBMV beamformer has improved the ultrasound image quality consistently and strongly in simulated, phantom and clinical datasets. Effectively stabilizing the covariance matrix from the angular diversities, the technique alleviates the Black Box Region (BBR) artifacts that traditionally plagued ESBMV, especially in deep or low signal zones, where coherence loss is strong. Field II simulations were initially used to establish this trend whereby a steady increase in SSNR within the BBR was obtained as the measure of angular diversity was increased and hence SC's physical capacity in restoring signal integrity compromised due to phase distortions was confirmed. These results were followed by phantom studies using the CIRS 040GSE dataset, where the SC-ESBMV structure provided significantly more clear images of cysts and a more uniform background speckle than both conventional ESBMV and FC.

Transitioning to a clinical evaluation using a human carotid artery dataset provided definite proof of the robustness of the algorithm under realistic dynamic conditions. Whereas conventional adaptive beamforming regularly fails in shadowed areas near the vessel boundaries, SC-ESBMV images had a remarkably homogeneous lumen texture and continuous wall delineation of vessels. Notably, the artifacts and dark shadow zones proximal to the far wall (which so often make diagnostic information difficult to interpret in conventional ESBMV) were effectively suppressed. This in-vivo success is directly related to the optimized parameters in the phantom study, where a threshold of $\delta = 0.3$ correlated with a step of 15° compounded that gave the optimal compromise between B-mode backscatter (BBR) attenuation and contrast retention.

Moreover, the post-processing technique of soft-contrast (SC) not only reduced the prevalence of artifacts but also increased the spatial fidelity of the imaging system at the same time. Across all datasets, there was an improvement in lateral resolution, attributed to a complementary decrease in full-width at half-maximum (FWHM), an indicator of sharper point-spread behavior and improved delineation of anatomically adjacent structures. Finally, the combination of SC with the spatial-beam modulated method (ESBMV) guarantees that the BBR artefacts mitigation does not affect the speckle statistics and the structural finesse. The SC-enhanced ESBMV approach therefore represents an efficient advanced ultrasound imaging method, allowing a delicate balance between suppression of the artifacts and enhancement of the resolution, thus representing a consistent performance and allowing a smooth transition from controlled simulations to the real world clinical applications.

IX. CONCLUSION

This investigation addresses the need for a complete comparative assessment of full-circular (FC) and selective-circular (SC) strategies as a strategic solution to the quandary of BBR artifacts inherent to enhanced spatial beamforming with a minimum variance (ESBMV) methodology that has been a long-standing problem. The empirical evidence

ISSN (online): 2581-3048
Volume 10, Issue 2, pp 19-30, February-2026
https://doi.org/10.47001/IRJIET/2026.102004

suggests that, despite a marginal advantage in contrast-to-noise ratio (CNR), FC is insufficient to achieve signal fidelity recovery in phase-degraded regions and cannot produce a statistically significant elevation in signal-to-noise ratio (SSNR) in the BBR domain. On the other hand, the combination of SC and ESBMV is a powerful method to reduce the signal voids from BBR. By leveraging angular diversity, the proposed framework stabilizes the covariance matrix estimate and effectively fills synthetic signal dropouts with physically reasonable speckle texture, rather than relying on simple noise smoothing.

Quantitative results obtained from two types of datasets - simulated and experimental data - reinforce the effectiveness of the SC-ESBMV approach. Notably, increasing the angular density to seven compounded orientations led to a significant increase in the SSNR in the BBR, from a baseline value of 2.89 to 4.89, while simultaneously improving the lateral resolution from a reduction in FWHM by 30%. Nonetheless, the study identifies an intrinsic trade-off: the higher the angular diversity, the greater the BBR's suppressing effect, but the slower the CNR due to angular averaging. The data identify the best value of $\delta = 0.3$, which provides the best balance between providing sufficient structural delineation and homogeneity of the background (vs. aggressive truncation schemes).

Finally, although the current framework makes a significant contribution to the study's visibility in the near and mid-field, the inherent weakness in the deeper auditory areas, which are mostly influenced by acoustic attenuation, underscores the need for additional academic research. Potential improvements may include adaptive coherence weighting or machine-learning-informed optimization, and hence maintain stability in complicated and deeply nested tissue conditions.

Potential avenues of advancement, therefore, include the integration of adaptive coherence weighting algorithms and data-driven optimization for robustness in complex, depth-dependent acoustic situations. Such efforts will play a critical role in expanding the utility of the methodology for a wider range of clinical scenarios.

Beyond deterministic compounding, recent advances in generative modeling highlight the potential of data-driven approaches for synthetic-data augmentation and automatic parameter optimization [27].

In summary, this research establishes a sound basis for architecture to expand the clinical usefulness of sophisticated adaptive beamformers to prove the high-resolution imaging process as resilient and diagnostically useful even in acoustically challenging situations.

REFERENCES

[1] B. M. Asl and A. Mahloojifar, “Eigenspace-based minimum variance beamforming applied to medical ultrasound imaging,” *IEEE Transactions on Ultrasonics, Ferroelectrics, and Frequency Control*, vol. 57, no. 11, pp. 2381–2390, 2010.

[2] H. Hasegawa, “Image quality assessment and challenges in modern ultrafast ultrasound imaging,” *Journal of Medical Ultrasonics*, vol. 51, no. 1, pp. 1–15, 2024.

[3] O. M. H. Rindal, A. Rodriguez-Molares, and A. Austeng, “The dark region artifact in adaptive ultrasound beamforming,” *in Proc. IEEE Int. Ultrasonics Symp. (IUS)*, 2017, pp. 1–4.

[4] P.-C. Li and M.-L. Li, "Adaptive imaging using the generalized coherence factor," *IEEE transactions on ultrasonics, ferroelectrics, and frequency control*, vol. 50, no. 2, pp. 128-141, 2003.

[5] R. Mallart and M. Fink, "The van Cittert–Zernike theorem in pulse echo measurements," *The Journal of the Acoustical Society of America*, vol. 90, no. 5, pp. 2718-2727, 1991.

[6] X. Zeng, C. Chen, and Y. Wang, "Eigenspace-based minimum variance beamformer combined with Wiener postfilter for medical ultrasound imaging," *Ultrasonics*, vol. 52, no. 8, pp. 996-1004, 2012.

[7] Y. Wang, C. Zheng, H. Peng, and X. Chen, “Short-lag spatial coherence combined with ESBMV beamformer for synthetic aperture ultrasound imaging,” *Computers in Biology and Medicine*, vol. 91, pp. 267–276, 2017.

[8] Z. Rami Alomari, Plane Wave Imaging Beamforming Techniques for Medical Ultrasound Imaging, Ph.D. Thesis, University of Leeds, 2017.

[9] Z. Lan, C. Zheng, Y. Wang, H. Peng, and H. Qiao, “Adaptive threshold for ESBMV beamformer for dark region artifacts elimination,” *IEEE Transactions on Instrumentation and Measurement*, vol. 70, pp. 1–16, 2021.

[10] J. Zhao, Y. Wang, J. Yu, W. Guo, T. Li, and Y.-P. Zheng, “Adaptive subarray coherence–based postfilter for eigenspace-based minimum variance beamforming in plane-wave imaging,” *Ultrasonics*, vol. 139, 2024.

[11] X. Li, P. Wang, and Q. Li, “Frequency-domain eigenspace projection minimum variance beamforming for ultrasound imaging,” *in Proceedings of the IEEE Signal Processing in Medicine and Biology Symposium (SPMB)*, 2025.

[12] C.-C. Shen, C.-H. Chen, and S.-L. Chen, “Improvement in multi-angle plane-wave image quality using delay-multiply-and-sum beamforming,” *Sensors*, vol. 24, no. 2, 2024.

ISSN (online): 2581-3048
Volume 10, Issue 2, pp 19-30, February-2026
https://doi.org/10.47001/IRJIET/2026.102004

[13] J.-F. Synnevåg, A. Austeng, and S. Holm, "Benefits of minimum-variance beamforming in medical ultrasound imaging," *IEEE Transactions on Ultrasonics, Ferroelectrics, and Frequency Control*, vol. 56, no. 9, pp. 1868–1879, 2009.

[14] Y. Li, Y. Winetraub, O. Liba, A. de la Zerda, and S. Chu, "Optimization of the trade-off between speckle reduction and axial resolution in frequency compounding," *IEEE Transactions on Medical Imaging*, vol. 38, no. 1, pp. 107–112, 2018.

[15] X. Wu, Q. Gao, M. Lu, T. Wang, and S. Chen, "An improved spatio-temporally smoothed coherence factor combined with ESBMV beamformer for plane-wave imaging," *in Proceedings of the IEEE International Ultrasonics Symposium (IUS)*, 2017, pp. 1–4.

[16] W. Wang, Q. He, Z. Zhang, and Z. Feng, "Adaptive beamforming using deep neural networks for ultrafast ultrasound imaging," *Ultrasonics*, vol. 126, p. 106823, 2022.

[17] G. Montaldo et al., "Coherent plane-wave compounding for very high frame rate ultrasonography," *IEEE Trans. UFFC*, 2009.

[18] P. N. T. Wells, "Ultrasonic imaging of the human body," *Reports on Progress in Physics*, 2006.

[19] J. Zhao et al., "Objective Image Quality Assessment for Adaptive Ultrasound Beamforming: Metrics and Benchmarks," *IEEE Access*, vol. 12, pp. 45210-45225, 2024.

[20] S. J. Kim and M. L. Oelze, "Quantitative Assessment of Lateral Resolution and Mainlobe Properties in Advanced Beamforming," *Ultrasound in Medicine & Biology*, vol. 49, no. 8, pp. 1842-1856, 2023.

[21] M. Jakovljevic et al., "Contrast-to-Noise Ratio Re-evaluated in the Era of Modern Ultrasound Beamforming," *IEEE Transactions on Medical Imaging*, vol. 41, no. 5, pp. 1105-1118, 2022.

[22] A.Rodriguez-Molares et al., "The Ultrasound Beamforming Toolbox: A Modern Framework for Image Quality Assessment," *IEEE Transactions on UFFC*, vol. 68, no. 6, pp. 2100-2115, 2021.

[23] J. A. Jensen, "Field II: A Program for Simulating Ultrasound Systems," *Medical & Biological Engineering & Computing*, vol. 34, pp. 351-353, 1996. [Online]. Available: https://field-ii.dk/

[24] Sun Nuclear (CIRS), "Multi-Purpose, Multi-Tissue Ultrasound Phantom Model 040GSE," *Technical Specifications*, 2023. [Online]. Available: https://www.sunnuclear.com/products/multi-purpose-multi-tissue-ultrasound-phantom

[25] H. Liebgott, A. Rodriguez-Molares, et al., "Plane-Wave Imaging Challenge in Medical Ultrasound (PICCmus)," *IEEE International Ultrasonics Symposium (IUS)*, 2016. [Online]. Available: https://www.creatis.insa-lyon.fr/Challenge/IEEE_IUS_2016/

[26] "IEEE Data Repository – Carotid Artery Plane-Wave Dataset," *IEEE Xplore*, 2016. [Online]. Available: https://ieeexplore.ieee.org/abstract/document/7728908

[27] H. ALHAJI and A. Y. Taqa, "Leveraging GANs and Vision Transformers for Text-to-Image Synthesis", *Iraqi Journal of Science*, vol. 67, no. 1, pp. 524–537, Jan. 2026, doi: 10.24996/ijs.2026.67.1.41.

AUTHORS BIOGRAPHY

Afnan Asaad is a M.Sc. candidate in Communication Engineering. She received her B.Sc. degree from the University of Ninevah in 2021. Her research interests include signal processing, image quality enhancement, and medical ultrasound imaging. Email: afnan.saeed2017@stu.uoninevah.edu.iq

Asst. Prof. Dr. Zainab R. Alomari is a faculty in the Department of Communications, Ninevah University. She has received her Ph.D. from Leeds University, where she worked with the ultrasound group on developing beamforming algorithms for ultrafast ultrasound imaging. Recently she is giving lectures for B.Sc. students on Microprocessors, DSP and MatlabLabs., supervising M.Sc. students under the subject of ultrasound imaging beamforming techniques, and doing research in thezainab.saleh@uoninevah.edu.iq

International Research Journal of Innovations in Engineering and Technology (IRJIET)

ISSN (online): 2581-3048

Volume 10, Issue 2, pp 19-30, February-2026

https://doi.org/10.47001/IRJIET/2026.102004

Citation of this Article:

Afnan Asaad, & Zainab R. Alomari. (2026). Reducing Black Box Region in ESBMV: A Comparative Study of Frequency and Spatial Compounding. *International Research Journal of Innovations in Engineering and Technology - IRJIET*, 10(2), 19-30. Article DOI https://doi.org/10.47001/IRJIET/2026.102004

****

